Journal of Sound and Vibration (1993) **160**(3), 433–454

NON-LINEAR DYNAMICS AND INSTABILITY OF A ROTATING SHAFT–DISK SYSTEM

C. O. CHANG AND J. W. CHENG

Institute of Applied Mechanics, National Taiwan University, Taipei, Taiwan, People's Republic of China

(*Received* 21 *August* 1990, *and in final form* 13 *September* 1991)

The instability and non-linear dynamics of a slender rotating shaft with a rigid disk at the mid-span are analyzed. The shaft is simply supported at both ends and is made of a viscoelastic material. The stability criteria are determined from the linear equations of motion based on the small strain assumption. The bifurcation of the double zero eigenvalue point on the stability boundaries in the parametric space is analyzed by using center manifold theory on the non-linear equations of motion, for which a large transverse displacement of the shaft is assumed. Analytical expressions for the radius of synchronous whirling and the radius and precession rate of non-synchronous whirling near the double zero eigenvalue point are obtained explicitly. The behaviors of the parameteric points away from the stability boundaries are analyzed numerically. The general effects on the precession rate for these points are somewhat different from those for the parametric points in the vicinity of the double zero eigenvalue.

1. INTRODUCTION

Among the components of machines designed to transmit power the most important are the shafts, or the shaft–disk assemblies. Kimball [1] found by experiment that internal damping destabilizes the whirling motion if the rotating speed of the rotor is higher than the critical speed. In references [2–8] the instability caused by internal damping has been examined theoretically. Ehrich [3] treated a continuous shaft without a lumped mass rotor and found that a particular whirl mode, which is not necessarily the fundamental mode, is induced for various values of internal damping. Bucciarelli [6] gave a clear picture of how internal forces can act to produce instability by coupling the motion of spin with the motion of whirl. Zhang and Ling [7] analyzed a rotating shaft which is non-uniform in cross-section and is made of a Boltzmann viscoelastic solid. Hendricks [8] investigated the rotor dynamics problem in which the shaft is made of a three-parameter model solid and its mass is neglected. Besides determining of the stability criteria, he found that a spiral motion evolves on a long time scale, governed by the viscoelastic time constant. The analysis in all the above-mentioned papers is based on the linear equations of motion. Meirovitch and Ryland [9] proposed a perturbation technique for the solution of a linear shaft–disk system with small internal and external damping.

The subject of this paper is to examine the non-linear dynamic behavior of a simple disk mounted at the middle of a uniform flexible shaft, made of a Kelvin model viscoelastic material. The shaft is simply supported and rotates at a constant speed. The external damping is assumed to be linear and uniformly distributed along the longitudinal axis of the shaft. The non-linearity results from the large transverse displacement of the shaft. Although Bolotin [2] made a non-linear study, he neglected the inertial terms of the shaft and assumed the length of the shaft to be inextensible. The non-linear damping forces from the bearings are not considered in the present analysis.

0022-460X/93/030433+22 $08.00/0 © 1993 Academic Press Limited

Hamilton's principle is used to derive the equations of motion. The Galerkin method is applied to yield an infinite set of coupled ordinary differential equations. The stability criteria are obtained, based on the truncated two-term linearized equations. Analysis for the double zero eigenvalue bifurcation is carried out by using center manifold theory. The behavior of the parametric points away from the stability boundaries is analyzed numerically.

2. EQUATIONS OF MOTION

The configuration of a simple shaft–disk assembly is shown in Figure 1. The slender shaft of undeformed length l, density ρ, circular cross-section area A and moment of inertia of the cross-section I rotates at a constant speed Ω. The co-ordinates x, y and z rotate at a constant spin rate Ω about the x axis, which passes through the longitudinal axis of the undeformed shaft. The assumption that the torsional motion, the longitudinal inertia, the shear deformation of the shaft, and gravity are neglected is made. Let P be an arbitrary point of the beam in the undeformed state and its position vector be $\vec{OP} = x\mathbf{i} + y\mathbf{j} + z\mathbf{k}$, where $\mathbf{i}$, $\mathbf{j}$ and $\mathbf{k}$ are the unit vectors of the x, y and z co-ordinate system. The point P is displaced to the point P' in the deformed state. The components of displacement of the neutral axis are denoted by $u(x, t)$, $v(x, t)$ and $w(x, t)$. By employing Euler beam theory and assuming small u', v' and w' [10], where a prime denotes differentiation with respect to x, the components (U, V, W) of the displacement of the point P along the x, y and z co-ordinates is found to be

$$U = u - zw' - yv', \qquad V = v, \qquad W = w. \tag{1a–c}$$

The non-linear terms in the Lagrangian strain–displacement equations are retained to account for the non-linearity induced by the fixed length requirement. It can be shown [11] that the only non-zero strain component is

$$\varepsilon_{xx} = u' - zw'' - yv'' + \tfrac{1}{2}(u')^2 + \tfrac{1}{2}(v')^2 + \tfrac{1}{2}(w')^2. \tag{2}$$

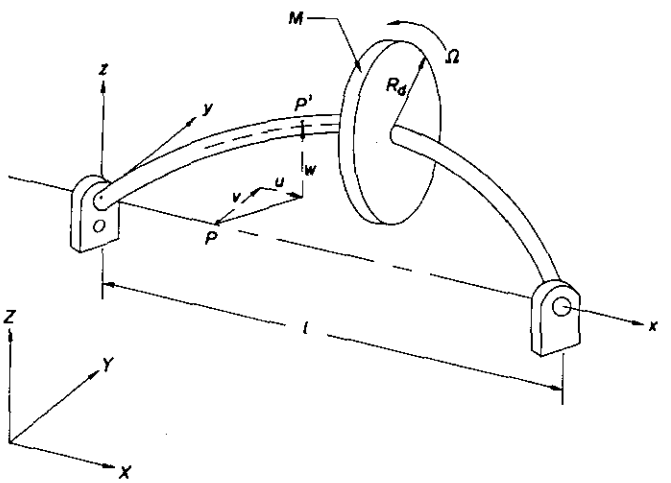

Figure 1. The rotating shaft–disk system.

Since the longitudinal motion is assumed to be small, the term $\frac{1}{2}(u')^2$ will be deleted. The equations of motion can be derived by using the extended Hamilton's principle [12, 13]

$$\int_0^t \{\delta T + \delta W_e - \delta \mathscr{V}\}\, \mathrm{d}t = 0, \tag{3}$$

where T is the total kinetic energy, δW_e is the virtual work done by the external forces and $\mathscr{V}$ is the strain energy. If the body is perfectly elastic, $\mathscr{V} = \int_V [\frac{1}{2}(\lambda + \frac{2}{3}\mu)(\varepsilon_{kk})^2 + \mu \varepsilon_{ij}\varepsilon_{ij}]\, \mathrm{d}V$ where λ and μ are the Lamé elastic constants, and τ_{ij} and ε_{ij} are the ijth components of the stress and strain tensors, respectively. If the elastic body has internal damping, such as that of a viscoelastic body, the explicit form of $\mathscr{V}$ is, in general, difficult to find. For such a case the last term within braces in equation (3) can be expressed in the variational form $\delta \mathscr{V} = \int_V \tau_{ij} \delta \varepsilon_{ij}\, \mathrm{d}V$, and the equations of motion can be derived, based on Hamilton's principle, without knowledge of the strain energy function once the stress–strain relationship is given [13].

The velocity of the point P' is

$$\dot{\mathbf{r}} = (\dot{\mathbf{r}})_{xyz} + \Omega \mathbf{i} \times \mathbf{r} = [\dot{u} - z\dot{w}' - y\dot{v}']\mathbf{i} + [\dot{v} - \Omega(z+w)]\mathbf{j} + [\dot{w} + \Omega(y+v)]\mathbf{k}. \tag{4}$$

The kinetic energy of the shaft–disk system is

$$T = \tfrac{1}{2} \int_V \rho(x) \dot{\mathbf{r}} \cdot \dot{\mathbf{r}}\, \mathrm{d}V = \tfrac{1}{2} \int_V \left[\rho + M\delta\left(x - \frac{l}{2}\right)\right] \dot{\mathbf{r}} \cdot \dot{\mathbf{r}}\, \mathrm{d}V, \tag{5}$$

where M is the mass of the disk and δ is the Dirac delta function. The substitution of equation (4) into equation (5) yields

$$\begin{aligned} T = {} & \frac{\rho}{2} \int_0^l [A\dot{u}^2 + I(\dot{w}')^2 + I(\dot{v}')^2 + A\dot{v}^2 + A\Omega^2 w^2 - 2A\Omega w\dot{v} + A\dot{w}^2 + A\Omega^2 v^2 + 2A\Omega v\dot{w}]\, \mathrm{d}x \\ & + \frac{M}{2} \int_0^l \delta\left(x - \frac{l}{2}\right)[\dot{u}^2 + \dot{v}^2 + \Omega^2 w^2 - 2\Omega w\dot{v} + \dot{w}^2 + \Omega^2 v^2 + 2\Omega v\dot{w}^2]\, \mathrm{d}x \\ & + \frac{I_d}{2} \int_0^l \delta\left(x - \frac{l}{2}\right)[(\dot{w}')^2 + (\dot{v}')^2]\, \mathrm{d}x + (\rho I l \Omega^2 + I_d \Omega^2), \end{aligned} \tag{6}$$

where $I_d = MR_d^2/4$ and R_d is the radius of the disk. Assume that the linear, uniformly distributed external damping force with damping coefficient μ_e is proportional to the velocity $\mathbf{r}_1$ of the neutral axis. Then the term δW_e in equation (3) is

$$\delta W_e = \int_0^l -\mu_e \mathbf{r}_1 \cdot \delta \mathbf{r}_1\, \mathrm{d}x = -\int_0^l \mu_e[(\dot{v} - \Omega w)\, \delta v + (\dot{w} + \Omega v)\, \delta w]\, \mathrm{d}x, \tag{7}$$

where $-\mu_e \mathbf{r}_1$ is the external damping force per unit length, equation (4) with $y = z = 0$ has been used, and the axial damping term $-\mu_e \dot{u}$ has been neglected. At low stress metals display a form of linear internal damping [14]. A viscoelastic model had been used to characterize the internal damping of the rotor constructed from metal by Ehrich [3] and Torby [5]. When a rotor is considered rotating at low speed and bears a light load, new materials such as polymers, plastics and composite materials, which possess relatively strong damping, may be used for the rotor; these materials have viscoelastic behavior. In references [7, 8] the effect of viscoelasticity on the vibration of a rotor has been studied. For simplicity, in this paper the shaft is assumed to be made of a Kelvin material with the

constitutive equation $\tau = E(\varepsilon + \mu_i \dot{\varepsilon})$, where E is the Young's elastic modulus and μ_i represents the internal damping coefficient. By integrating by parts, using the geometrical boundary conditions $u = v = w = 0$ at $x = 0, l$, and assuming no external force in the x direction, equation (3) can be put in the form [15]

$$\int_0^t \left\{ EI(w'' + \mu_i \dot{w}'')\delta w'|_0^l + EI(v'' + \mu_i \dot{v}'')\delta v'|_0^l - \int_0^l [(\cdots)\delta u + (\cdots)\delta v + (\cdots)\delta w]\,\mathrm{d}x \right\} \mathrm{d}t = 0. \tag{8}$$

From equation (8) one obtains the natural boundary conditions

$$w'' = -\mu_i \dot{w}'', \quad v'' = -\mu_i \dot{v}'', \qquad \text{at } x = 0, l. \tag{9}$$

For a practical viscoelastic material μ_i is very small: i.e., $\mu_i \ll 1$. On the assumption of small μ_i equation (9) becomes $v'' \approx 0$ and $w'' \approx 0$. So the natural boundary conditions of the simply supported non-rotational beam are used in the rest of the paper. Since δu is arbitrary for $0 < x < l$, this leads to the condition that the coefficient of δu in equation (8) must be zero, which in turn give the equation of motion for the x component,

$$G' = [u' + \tfrac{1}{2}((v')^2 + (w')^2) + \mu_i \dot{u}' + \mu_i (v'\dot{v}' + w'\dot{w}')]' = 0, \tag{10}$$

where $(\,)' = \partial(\,)/\partial x$. From equation (10) one knows that G is independent of x and can be expressed as

$$G(t) = \frac{1}{l} \int_0^l G\,\mathrm{d}x. \tag{11}$$

By letting the coefficients of δv and δw in equation (8) equal zero and using equation (11) and the conditions $u = \dot{u} = 0$ at $x = 0, l$, the other two equations of motion are found to be

$$[\rho A + M\delta(x - l/2)](\ddot{v} - 2\Omega\dot{w} - \Omega^2 v) - I_d[\delta'(x - l/2)\ddot{v}' + \delta(x - l/2)\ddot{v}''] + \mu_i \dot{v} - \mu_e \Omega w + EIv'''' + EI\mu_i \dot{v}'''' - \frac{EA}{2l}\left\{ \int_0^l [(v')^2 + (w')^2]\,\mathrm{d}x + \mu_i \frac{\mathrm{d}}{\mathrm{d}t} \int_0^l [(v')^2 + (w')^2]\,\mathrm{d}x \right\} v'' = 0, \tag{12a}$$

$$[\rho A + M\delta(x - l/2)](\ddot{w} + 2\Omega\dot{v} - \Omega^2 w) - I_d[\delta'(x - l/2)\ddot{w}' + \delta(x - l/2)\ddot{w}''] + \mu_e \dot{w} + \mu_e \Omega v + EIw'''' + EI\mu_i \dot{w}'''' - \frac{EA}{2l}\left\{ \int_0^l [(v')^2 + (w')^2]\,\mathrm{d}x + \mu_i \frac{\mathrm{d}}{\mathrm{d}t} \int_0^l [(v')^2 + (w')^2]\,\mathrm{d}x \right\} w'' = 0, \tag{12b}$$

where $\delta' = \mathrm{d}\delta/\mathrm{d}x$. The differential–integral equations (12a) and (12b) are coupled in v and w but uncoupled in u. The solution of equation (12) is assumed in the form

$$v(x, t) = \sum_{k=1}^{\infty} \phi_k(x) v_k(t), \qquad w(x, t) = \sum_{k=1}^{\infty} \phi_k(x) w_k(t), \tag{13a, b}$$

where $\phi_k = \sqrt{2} \sin(k\pi x/l)$, which are the eigenfunctions of the linear equations of a simply supported non-rotating beam. The substitution of equation (13) into equation (12) and the use of Galerkin's method yield the following set of non-linear ordinary differential

equations:

$$\rho Al(\ddot{v}_n - 2\Omega\dot{w}_n - \Omega^2 v_n) + EI l\Omega_n^2(v_n + \mu_i\dot{v}_n) + \mu_e l(\dot{v}_n - \Omega w_n)$$
$$+\frac{EAl}{2}\left\{\left(1+\mu_i\frac{\mathrm{d}}{\mathrm{d}t}\right)\left[\sum_{j=1}^{\infty}(v_j^2+w_j^2)\Omega_j\right]\right\}\Omega_n v_n \tag{14a}$$
$$+2M\sum_{k=1}^{\infty}\sin\frac{k\pi}{2}(\ddot{v}_k - 2\Omega\dot{w}_k - \Omega^2 v_k)\sin\frac{n\pi}{2} + 2I_d\sum_{k=1}^{\infty}\left[\frac{kn\pi^2}{l^2}\cos\frac{k\pi}{2}\cos\frac{n\pi}{2}\right]\ddot{v}_k = 0,$$

$$\rho Al(\ddot{w}_n + 2\Omega\dot{v}_n - \Omega^2 w_n) + EI l\Omega_n^2(w_n + \mu_i\dot{w}_n) + \mu_e l(\dot{w}_n - \Omega v_n)$$
$$+\frac{EAl}{2}\left\{\left(1+\mu_i\frac{\mathrm{d}}{\mathrm{d}t}\right)\left[\sum_{j=1}^{\infty}(v_j^2+w_j^2)\Omega_j\right]\right\}\Omega_n w_n \tag{14b}$$
$$+2M\sum_{k=1}^{\infty}\sin\frac{k\pi}{2}(\ddot{w}_k + 2\Omega\dot{v}_k - \Omega^2 w_k)\sin\frac{n\pi}{2} + 2I_d\sum_{k=1}^{\infty}\left[\frac{kn\pi^2}{l^2}\cos\frac{k\pi}{2}\cos\frac{n\pi}{2}\right]\ddot{w}_k = 0,$$

where $n=1, 2, 3, \ldots, \Omega_n=(n\pi/l)^2$. Noted that in the derivation of equation (14) one uses the orthogonality of the eigenvalues, $\int_0^l \phi_k\phi_s\,\mathrm{d}x=0$ if $k\neq s$, $\int_0^l \phi_k\phi_s\,\mathrm{d}x\neq 0$ if $k=s$, and by using integration by parts the terms involving the derivative of the delta function can be expressed as $\int_0^l \delta'(x-l/2)v_k(t)\phi_k\,\mathrm{d}x=\delta(x-l/2)v_k(t)\phi_k|_0^l-\int_0^l\delta(x-l/2)v_k(t)\phi_k'\,\mathrm{d}x$. The gyroscopic effects of the rotating disk appear in the even modes: i.e., $n=2, 4, \ldots$ Since the amplitudes of the high order modes are small, only the approximate equations resulting from the truncated first two modes are analyzed. By introducing the non-dimensional quantities

$$\hat{v}_n=v_n/l, \quad \hat{w}_n=w_n/l, \quad \hat{x}=x/l, \quad \hat{\Omega}_n=\Omega_n l^2, \quad \hat{\mathscr{J}}_d=I_d/\rho Al^3, \quad \hat{\mathscr{M}}=M/\rho Al,$$
$$\tau=\sqrt{EI/\rho Al^4}\,t=\nu t, \quad \hat{\Omega}=\Omega/\nu, \quad \hat{\mu}_i=\mu_i\nu, \quad \hat{\mu}_e=\mu_e/\rho A\nu, \quad \alpha=Al^2/2I,$$

where $\hat{\Omega}_n$ is the nth dimensionless natural frequency of a simply supported non-rotational beam, equations (14) for $n=1, 2$ with all over-hats dropped for convenience can be recast in dimensionless form as

$$\left[1+2\mathscr{M}\sin^2\frac{n\pi}{2}\right](\ddot{v}_n - 2\Omega\dot{w}_n - \Omega^2 v_n) + 2\mathscr{J}_d\Omega_n\cos^2\frac{n\pi}{2}\ddot{v}_n + \Omega_n^2(v_n+\mu_i\dot{v}_n)$$
$$+\mu_e(\dot{v}_n - \Omega w_n) + \alpha\Omega_n\left\{\left(1+\mu_i\frac{\mathrm{d}}{\mathrm{d}\tau}\right)\left[\sum_{j=1}^{2}(v_j^2+w_j^2)\Omega_j\right]\right\}v_n = 0, \tag{15a}$$

$$\left[1+2\mathscr{M}\sin^2\frac{n\pi}{2}\right](\ddot{w}_n + 2\Omega\dot{v}_n - \Omega^2 w_n) + 2\mathscr{J}_d\Omega_n\cos^2\frac{n\pi}{2}\ddot{w}_n + \Omega_n^2(w_n+\mu_i\dot{w}_n)$$
$$+\mu_e(\dot{w}_n - \Omega v_n) + \alpha\Omega_n\left\{\left(1+\mu_i\frac{\mathrm{d}}{\mathrm{d}\tau}\right)\left[\sum_{j=1}^{2}(v_j^2+w_j^2)\Omega_j\right]\right\}w_n = 0, \tag{15b}$$

where $n=1, 2$ and $(\dot{\ })=\mathrm{d}(\ )/\mathrm{d}\tau$.

In order to facilitate the non-linear analysis by using center manifold theory [16], equations (15) have to be reorganized in the form of first order ordinary differential

equations. Denote

$$\mathbf{y}=(\mathbf{y}_1^{\mathrm{T}},\mathbf{y}_2^{\mathrm{T}})^{\mathrm{T}}=(y_1,y_2,y_3,y_4,y_5,y_6,y_7,y_8)^{\mathrm{T}}=(v_1,w_1,\dot{v}_1,\dot{w}_1,v_2,w_2,\dot{v}_2,\dot{w}_2)^{\mathrm{T}},$$

$$\bar{\Omega}=\Omega_1/\sqrt{1+2\mathscr{M}},\ \text{and}\ \bar{\Omega}_2=\Omega_2/\sqrt{1+2\mathscr{J}_d\Omega_2}.$$

Then equations (15) can be expressed as

$$\dot{\mathbf{y}}_1=\mathbf{C}_1\mathbf{y}_1+\mathbf{n}_1(\mathbf{y}_1,\mathbf{y}_2),\qquad \dot{\mathbf{y}}_2=\mathbf{C}_2\mathbf{y}_2+\mathbf{n}_2(\mathbf{y}_1,\mathbf{y}_2),\tag{16a, b}$$

where

$$\mathbf{C}_1=\begin{bmatrix} 0 & 0 & 1 & 0\\ 0 & 0 & 0 & 1\\ \Omega^2-\bar{\Omega}_1^2 & \dfrac{\mu_e\Omega}{1+2\mathscr{M}} & -\mu_i\bar{\Omega}_1^2-\dfrac{\mu_e}{1+2\mathscr{M}} & 2\Omega\\ \dfrac{-\mu_e\Omega}{1+2\mathscr{M}} & \Omega^2-\bar{\Omega}_1^2 & -2\Omega & -\mu_i\bar{\Omega}_1^2-\dfrac{\mu_e}{1+2\mathscr{M}} \end{bmatrix},\tag{17a}$$

$$\mathbf{C}_2=\begin{bmatrix} 0 & 0 & 1 & 0\\ 0 & 0 & 0 & 1\\ \dfrac{\Omega^2}{1+2\mathscr{J}_d\Omega_2}-\bar{\Omega}_2^2 & \dfrac{\mu_e\Omega}{1+2\mathscr{J}_d\Omega_2} & -\mu_i\bar{\Omega}_2^2-\dfrac{\mu_e}{1+2\mathscr{J}_d\Omega_2} & \dfrac{2\Omega}{1+2\mathscr{J}_d\Omega_2}\\ \dfrac{-\mu_e\Omega}{1+2\mathscr{J}_d\Omega_2} & \dfrac{\Omega^2}{1+2\mathscr{J}_d\Omega_2}-\bar{\Omega}_2^2 & \dfrac{-2\Omega}{1+2\mathscr{J}_d\Omega_2} & -\mu_i\bar{\Omega}_2^2-\dfrac{\mu_e}{1+2\mathscr{J}_d\Omega_2} \end{bmatrix},\tag{17b}$$

and $\mathbf{n}_1=(N_1,N_2,N_3,N_4)^{\mathrm{T}}$ and $\mathbf{n}_2=(N_5,N_6,N_7,N_8)^{\mathrm{T}}$ with

$$N_1=N_2=N_5=N_6=0,$$

$$N_3=-\alpha\bar{\Omega}_1^2(y_1^3+y_1y_2^2)-\frac{\alpha\Omega_1\Omega_2}{1+2\mathscr{M}}(y_1y_5^2+y_1y_6^2)-2\mu_i\alpha\bar{\Omega}_1^2y_1(y_1y_3+y_2y_4)$$
$$-\frac{2\mu_i\alpha\Omega_1\Omega_2y_1}{1+2\mathscr{M}}(y_5y_7+y_6y_8),$$

$$N_4=-\alpha\bar{\Omega}_1^2y_2(y_1y_2+y_2^2)-\frac{\alpha\Omega_1\Omega_2}{1+2\mathscr{M}}y_2(y_5^2+y_6^2)-2\mu_i\alpha\bar{\Omega}_1^2y_2(y_1y_3+y_2y_4)$$
$$-\frac{2\mu_i\alpha\Omega_1\Omega_2}{1+2\mathscr{M}}y_2(y_5y_7+y_6y_8),$$

$$N_7=-\frac{\alpha\Omega_1\Omega_2}{1+2\mathscr{J}_d\Omega_2}y_5(y_1^2+y_2^2)-\alpha\bar{\Omega}_2^2y_5(y_5^2+y_6^2)-\frac{2\mu_i\alpha\Omega_1\Omega_2}{1+2\mathscr{J}_d\Omega_2}y_5(y_1y_3+y_2y_4)$$
$$-2\mu_i\alpha\bar{\Omega}_2^2y_5(y_5y_7+y_6y_8),$$

$$N_8=-\frac{\alpha\Omega_1\Omega_2}{1+2\mathscr{J}_d\Omega_2}y_6(y_1^2+y_2^2)-\alpha\bar{\Omega}_2^2y_6(y_5^2+y_6^2)-\frac{2\alpha\mu_i\Omega_1\Omega_2}{1+2\mathscr{J}_d\Omega_2}y_6(y_1y_3+y_2y_4)\tag{17c}$$
$$-2\mu_i\alpha\bar{\Omega}_2^2y_6(y_5y_7+y_6y_8).$$

3. LINEAR ANALYSIS

The existence and stability of steady state solutions are discussed in this section. It is easy to see that the trivial solution $\mathbf{y}=0$ corresponding to the undeformed rotation of a shaft is a solution of equation (16). By linearizing equation (16) about the trivial solution one obtains

$$\dot{\mathbf{y}}_1=\mathbf{C}_1\mathbf{y}_1, \qquad \dot{\mathbf{y}}=\mathbf{C}_2\mathbf{y}_2. \tag{18a, b}$$

Equations (18) can also be obtained from the equations of motion which have the non-linear terms $\frac{1}{2}[(u')^2+(v')^2+(w')^2]$ of equation (3) dropped. It can be found that equations (18) are uncoupled for variables $\mathbf{y}_1$ and $\mathbf{y}_2$ and have no non-trivial steady state solution. To determine the stability of the trivial solution, the solution of equation (18a) is assumed as

$$\mathbf{y}_1=\mathbf{a}_1\,e^{\lambda\tau}. \tag{19}$$

Substitution of equation (19) into equation (18a) yields the characteristic equation

$$\lambda^4+\bar{C}_1\lambda^3+\bar{C}_2\lambda^2+\bar{C}_3\lambda+\bar{C}_4=0, \tag{20}$$

where

$$\bar{C}_1=(2\mu_e\tilde{M}+2\mu_i\tilde{M}\Omega_1^2)/\tilde{M}^2, \qquad \bar{C}_2=(\mu_e^2+2\mu_i\mu_e\Omega_1^2+2\tilde{M}\Omega_1^2+\mu_i^2\Omega_1^4+2\tilde{M}^2\Omega^2)/\tilde{M}^2,$$

$$\bar{C}_3=(2\mu_e\Omega_1^2+2\mu_i\Omega_1^4+2\mu_e\tilde{M}\Omega^2-2\mu_i\tilde{M}\Omega_1^2\Omega^2)/\tilde{M}^2,$$

$$\bar{C}_4=(\Omega_1^4+\mu_e^2\Omega^2-2\tilde{M}\Omega_1^2\Omega^2+\tilde{M}^2\Omega^4)/\tilde{M}^2,$$

and $\tilde{M}=1+2\mathscr{M}$.

According to the Routh–Hurwitz criterion the system (18a) is stable if the condition $\bar{C}_1\bar{C}_2\bar{C}_3-\bar{C}_3^2-\bar{C}_1^2\bar{C}_4>0$ holds. In terms of the system parameters, and through the use of the Mathematica software package [17] for simplification, the stable condition can be expressed as

$$\Omega_1^2(\mu_e^2+2\mu_e\mu_i\Omega_1^2+\mu_i^2\Omega^4+4\tilde{M}^2\Omega^2)[(\mu_e+\mu_i\Omega_1^2)^2-\mu_i^2\tilde{M}\Omega_1^2\Omega^2]/\tilde{M}^5>0. \tag{21}$$

Condition (21) implies that

$$\Omega<(1/\sqrt{1+2\mathscr{M}})(\Omega_1+\mu_e/\mu_i\Omega_1)\equiv\Omega_1^*. \tag{22}$$

Similarly, the solution of equation (18b) is assumed as

$$\mathbf{y}_2=\mathbf{a}_2\,e^{\lambda_2\tau}. \tag{23}$$

Substituting equation (23) into equation (18b) gives the resulting characteristic equation as

$$\lambda_2^4+d_1\lambda_2^3+d_2\lambda_2^2+d_3\lambda_2+d_4=0, \tag{24}$$

where

$$d_1=(2\mu_e+2\mu_i\Omega_2^2)/\tilde{I}, \qquad d_2=(\mu_e^2+2\mu_i\mu_e\Omega_2^2+2\tilde{I}\Omega^2+\mu_i\Omega^4+2\Omega^2-2\tilde{I}\Omega^2)/\tilde{I}^2,$$

$$d_3=(2\mu_e\Omega_2^2+2\mu_i\Omega_2^4+2\mu_e\Omega^2-2\mu_i\Omega_2^2\Omega^2)/\tilde{I}^2, \qquad d_4=(\Omega^4+\mu_e^2\Omega^2-2\Omega_2^2\Omega^2+\Omega^4)/\tilde{I}^2,$$

and $\tilde{I}=1+2\mathscr{I}_d\Omega_2$.

Employing the Routh–Hurwitz criterion and using the Mathematica software package yields the criterion for stable motion as

$$(\mu_e^2+2\mu_e\mu_i\Omega_2^2+\mu_i^2\Omega_2^4+4\Omega^4)(\mu_e^2\Omega_2^2+2\mu_e\mu_i\Omega_2^4 +\mu_i^2\Omega_2^6+\mu_e^2\Omega^2-\mu_e^2\tilde{I}\Omega^2-\mu_i^2\Omega_2^4\Omega^2)/\tilde{I}^5>0. \tag{25}$$

Condition (25) implies that

$$\Omega<(\mu_e\Omega_2+\mu_i\Omega_2^3)/\sqrt{2\mu_e^2\mathscr{I}_d\Omega_2+\mu_i^2\Omega_2^4}\equiv\Omega_2^*. \tag{26}$$

The stable region is the intersection of equations (22) and (26). The effect of μ_e and μ_i on the stability criteria are summarized in the following.

(a) If $\mu_e\neq0$, equation (22) shows that the critical speed Ω_1^* approaches infinity as μ_i approaches zero. This means that the first mode motion is stable for any rotating speed Ω in the absence of internal damping. Furthermore, the larger μ_i, the smaller the critical speed; this means that internal damping destabilizes the first mode motion [2].

(b) If $\mu_e\neq0$, equation (26) shows that $\Omega_2^*\to\Omega_2^{1/2}/\sqrt{2\mathscr{I}_d}$, or Ω_2^* is proportional to $\Omega_2^{1/2}$ as $\mu_i\to0$; thus the critical speed Ω_2^* is proportional to Ω_2 as μ_i tends to infinity. This means that internal damping will improve the stability of the second mode motion.

(c) If $\mu_i\neq0$, decrease of external damping will decrease both Ω_1^* and Ω_2^*.

(d) If $\mu_e=0$, the critical speeds become $\Omega_1^*=\pi^2/\sqrt{1+2\mathscr{M}}=\bar{\Omega}_1$ and $\Omega_2^*=4\pi^2\equiv\Omega_2^{*0}$. It is clear that $\bar{\Omega}_1<\Omega_2^{*0}$. At the stability boundary, i.e., $\Omega=\bar{\Omega}_1$, the solution of equation (18b) is asymptotically stable and the eigenvalues of equation (18a) are

$$\lambda_{1,2}=0,0,\qquad \lambda_{3,4}=-\bar{\Omega}_1^2\mu_i\pm2\bar{\Omega}_1\mathrm{i}\equiv\xi\pm\eta\mathrm{i}. \tag{27}$$

Let $\mathbf{y}_1^1=\mathbf{b}_1=(b_1,b_2,b_3,b_4)^{\mathrm{T}}$ and $\mathbf{y}_1^2=\mathbf{b}_2\tau$ be the solutions corresponding to the double zero eigenvalues. Substituting them into equation (18a), one finds that $\mathbf{b}_2=\mathbf{0}$, $b_3=b_4=0$, and b_1 and b_2 are arbitrary. So the linearized equation (18) predicts that at the critical speed the shaft is in the first mode whirl and is neutrally stable. But if any one of the eigenvalues has a zero real part, the stability cannot be determined by linearization [18]; therefore this critical point will be re-examined based on the non-linear equation (16) in the next section.

Consider a specific example for which the parameters of the system are $l=1$ m, R (the radius of the shaft) $=0{\cdot}04$ m, h (the thickness of the disk) $=0{\cdot}1$ m, $R_d=0{\cdot}16$ m,

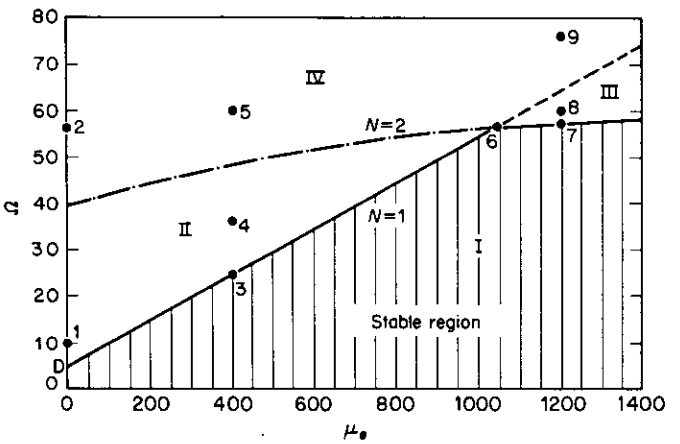

Figure 2. Stability boundaries in the Ω–μ_e plane.

$\rho = 7600\ \text{kg/m}^3$, $E = 190\ \text{GPa}$, $\mu_i = 0{\cdot}01$. Then the dimensionless quantities are $\hat{\mathscr{M}} = 1{\cdot}6$, $\hat{\mathscr{J}}_d = 0{\cdot}01024$, $\alpha = 1250$, $\nu = 100$, $\hat{\mu}_i = 1$ and $\hat{\mu}_e = \mu_e/3820$. The stability boundaries given by equations (22) and (26) are plotted in the Ω–μ_e plane in Figure 2. The point D in Figure 2 is of the double zero eigenvalue bifurcation point and Hopf bifurcations occur at all non-intersection points on the stability boundaries.

4. NON-LINEAR ANALYSIS

In this section the possible non-trivial steady state solutions and non-synchronous limit cycle solutions for the parameters Ω and μ_e outside the stable region of Figure 2 are investigated. A study of the eigenvalues of equations (20) and (24) reveals that for different values of Ω and μ_e double zero bifurcation, Hopf bifurcation, and double Hopf bifurcation can occur. The behavior of the rotating shaft–disk system near the bifurcation points is analyzed by center manifold theory and a numerical method.

4.1. NON-TRIVIAL STEADY STATE SOLUTIONS

To determine the non-trivial steady state solution the velocities and accelerations of v_1, w_1, v_2 and w_2 in equation (15) or (16) are set to zero; then equation (15) becomes

$$\left[\bar{\Omega}_1^2 - \Omega^2 + \alpha\bar{\Omega}_1^2 R_1^2 + \frac{\alpha\Omega_1\Omega_2}{1+2\mathscr{M}} R_2^2\right] v_1 - \frac{\mu_e\Omega}{1+2\mathscr{M}} w_1 = 0, \tag{28a}$$

$$\frac{\mu_e\Omega}{1+2\mathscr{M}} v_1 + \left[\bar{\Omega}_1^2 - \Omega^2 + \alpha\bar{\Omega}_1^2 R_1^2 + \frac{\alpha\Omega_1\Omega_2}{1+2\mathscr{M}} R_2^2\right] w_1 = 0, \tag{28b}$$

$$[\Omega_2^2 - \Omega^2 + \alpha\Omega_2(R_1^2\Omega_1 + R_2^2\Omega_2)] v_2 - \mu_e\Omega w_2 = 0, \tag{28c}$$

$$\mu_e\Omega v_2 + [\Omega_2^2 - \Omega^2 + \alpha\Omega_2(R_1^2\Omega_1 + R_2^2\Omega_2)] w_2 = 0, \tag{28d}$$

where

$$R_1^2 = v_1^2 + w_1^2, \qquad R_2^2 = v_2^2 + w_2^2. \tag{28e, f}$$

It can be shown that a non-trivial steady state solution of equations (28) does not exist if $\mu_e \neq 0$. If one assumes that equations (28) have a non-trivial steady state solution, then, from equations (28a) and (28b), one has

$$\frac{w_1}{v_1} = \frac{[(\bar{\Omega}_1^2 - \Omega^2 + \alpha\bar{\Omega}_1^2 R_1^2)(1+2\mathscr{M}) + \alpha\Omega_1\Omega_2 R_2^2]}{\mu_e\Omega}$$

$$= \frac{-\mu_e\Omega}{[(1+2\mathscr{M})(\bar{\Omega}_1^2 - \Omega^2 + \alpha\bar{\Omega}_1^2 R_1^2) + \alpha\Omega_1\Omega_2 R_2^2]};$$

this leads to the contradictory result

$$[(1+2\mathscr{M})(\bar{\Omega}_1^2 - \Omega^2 + \alpha\bar{\Omega}_1^2 R_1^2) + \alpha\Omega_1\Omega_2 R_2^2]^2 + (\mu_e\Omega)^2 = 0.$$

The same thing happens to equations (28c) and (28d). Therefore, non-trivial steady state solutions for $\mu_e \neq 0$ do not exist. If $\mu_e = 0$, in such a case $\Omega_1^* = \bar{\Omega}_1$ and $\Omega_2^* = \Omega_2^{*0} = \Omega_2$, and

equations (28) reduce to

$$\left[\bar{\Omega}_1^2-\Omega^2+\alpha\bar{\Omega}_1^2R_1^2+\frac{\alpha\Omega_1\Omega_2}{1+2\mathscr{M}}R_2^2\right]v_1=0,$$

$$\left[\bar{\Omega}_1^2-\Omega^2+\alpha\bar{\Omega}_1^2R_1^2+\frac{\alpha\Omega_1\Omega_2}{1+2\mathscr{M}}R_2^2\right]w_1=0, \tag{29a, b}$$

$$[\Omega_2^2-\Omega^2+\alpha\Omega_2(R_1^2\Omega_1+R_2^2\Omega_2)]v_2=0, \qquad [\Omega_2^2-\Omega^2+\alpha\Omega_2(R_1^2\Omega_1+R_2^2\Omega_2)]w_2=0, \tag{29c, d}$$

As can be seen from equations (29), for some ranges of Ω the following non-trivial steady state solutions may exist.

(1) If $\bar{\Omega}_1<\Omega<\Omega_2^{*0}$, one has $v_2=w_2=0$ from equations (29c) and (29d) and

$$R_1^2=v_1^2+w_1^2=(\Omega^2-\bar{\Omega}_1^2)/\alpha\bar{\Omega}_1^2, \tag{30}$$

from equations (29a) and (29b). Equation (30) indicates that the rotating shaft whirls at the first node.

(2) If $\Omega_2^{*0}<\Omega$, there are two non-trivial steady state solutions which may exist: that is,

$$R_1^2=v_1^2+w_1^2=(\Omega^2-\bar{\Omega}_1^2)/\alpha\bar{\Omega}_1^2, \qquad v_2=w_2=0, \tag{31a}$$

$$R_2^2=v_2^2+w_2^2=(\Omega^2-\Omega_2^2)/\alpha\Omega_2^2, \qquad v_1=w_1=0. \tag{31b}$$

Equations (31) indicate that the rotating shaft may whirl at either the first mode or the second mode. Which mode the shaft whirls at depends on the perturbed initial conditions and will be proved later on by the numerical solution.

4.2. DOUBLE ZERO EIGENVALUE BIFURCATION

In this subsection the bifurcation analysis near the point D shown in Figure 2 is performed. Let $\underline{\varepsilon}=(\varepsilon_1, \varepsilon_2)^T$, where $\varepsilon_1=\Omega-\bar{\Omega}_1$ and $\varepsilon_2=\mu_e$; these parameters measure the deviation of Ω and μ_e from the point D. The matrix $\mathbf{C}_1$ can be decomposed in terms of $\underline{\varepsilon}$ into

$$\mathbf{C}_1=\mathbf{C}_{10}+\mathbf{C}_{1\varepsilon}, \tag{32a}$$

where

$$\mathbf{C}_{10}=\begin{bmatrix}0 & 0 & 1 & 0\\ 0 & 0 & 0 & 1\\ 0 & 0 & -\mu_i\bar{\Omega}_1^2 & 2\bar{\Omega}_1\\ 0 & 0 & -2\bar{\Omega}_1 & -\mu_i\bar{\Omega}_1^2\end{bmatrix},$$

$$\mathbf{C}_{1\varepsilon}=\begin{bmatrix}0 & 0 & 0 & 0\\ 0 & 0 & 0 & 0\\ \varepsilon_1(2\bar{\Omega}_1+\varepsilon_1) & \dfrac{\varepsilon_2(\varepsilon_1+\bar{\Omega}_1)}{1+2\mathscr{M}} & -\dfrac{\varepsilon_2}{1+2\mathscr{M}} & 2\varepsilon_1\\ -\dfrac{\varepsilon_2(\varepsilon_1+\bar{\Omega}_1)}{1+2\mathscr{M}} & \varepsilon_1(2\bar{\Omega}_1+\varepsilon_1) & -2\varepsilon_1 & -\dfrac{\varepsilon_2}{1+2\mathscr{M}}\end{bmatrix}. \tag{32b, c}$$

Similarly, $\mathbf{C}_2$ can be decomposed into

$$\mathbf{C}_2=\mathbf{C}_{20}+\mathbf{C}_{21}+\mathbf{C}_{22}, \tag{33}$$

where $\mathbf{C}_{20}$ is independent of $\underline{\varepsilon}$, $\mathbf{C}_{21}$ is a linear function in $\underline{\varepsilon}$, and all the elements of $\mathbf{C}_{22}$ are proportional to $|\underline{\varepsilon}|^2$.

$\mathbf{C}_{10}$ has two zero eigenvalues and a pair of complex conjugate ones with negative real parts, as given in equations (27). All the eigenvalues of $\mathbf{C}_2$ have negative real parts in the neighborhood of the point D. Hence a codimension two bifurcation will occur [18]. Equation (16a) can be put into canonical form by introducing the change of co-ordinates $\mathbf{y}_1=\mathbf{Q}\mathbf{z}$ as

$$\dot{\mathbf{z}}=\mathbf{Q}^{-1}(\mathbf{C}_{10}+\mathbf{C}_{1\varepsilon})\mathbf{Q}\mathbf{z}+\mathbf{Q}^{-1}\mathbf{n}_1(\mathbf{Q}\mathbf{z}, \mathbf{y}_2), \tag{34}$$

where

$$\mathbf{Q}=\begin{bmatrix} 1 & 0 & 1/\lambda_3 & \mathrm{i}/\lambda_4 \\ 0 & 1 & \mathrm{i}/\lambda_3 & 1/\lambda_4 \\ 0 & 0 & 1 & \mathrm{i} \\ 0 & 0 & \mathrm{i} & 1 \end{bmatrix}, \qquad \mathbf{Q}^{-1}=\begin{bmatrix} 1 & 0 & -\xi/d & \eta/d \\ 0 & 1 & -\eta/d & -\xi/d \\ 0 & 0 & 1/2 & -\mathrm{i}/2 \\ 0 & 0 & -\mathrm{i}/2 & 1/2 \end{bmatrix}. \tag{35}$$

The columns of $\mathbf{Q}$ are the eigenfunctions of the matrix $\mathbf{C}_{10}$. In equations (35) λ_3 and λ_4 are given by equations (27) and $d=\xi^2+\eta^2$. Let $\mathbf{z}=(z_1, z_2, z_3, z_4)^{\mathrm{T}}$ and consider $\underline{\varepsilon}$ as a state variable vector. Equation (34) is expressed in the developed form as

$$\begin{Bmatrix} \dot{z}_1 \\ \dot{z}_2 \end{Bmatrix}=\begin{bmatrix} 0 & 0 \\ 0 & 0 \end{bmatrix}\begin{Bmatrix} z_1 \\ z_2 \end{Bmatrix}$$

$$+\begin{bmatrix} -\dfrac{\xi}{d}2\bar{\Omega}_1\varepsilon_1-\dfrac{\eta\bar{\Omega}_1}{d(1+2\mathscr{M})}\varepsilon_2+b_1 & \dfrac{\eta}{d}2\bar{\Omega}_1\varepsilon_1-\dfrac{\xi\bar{\Omega}_1}{d(1+2\mathscr{M})}\varepsilon_2+b_2 \\ -\dfrac{\eta}{d}2\bar{\Omega}_1\varepsilon_1+\dfrac{\xi\bar{\Omega}_1}{d(1+2\mathscr{M})}\varepsilon_2-b_2 & -\dfrac{\xi}{d}2\bar{\Omega}_1\varepsilon_1-\dfrac{\eta\bar{\Omega}_1}{d(1+2\mathscr{M})}\varepsilon_2+b_1 \end{bmatrix}\begin{Bmatrix} z_1 \\ z_2 \end{Bmatrix}$$

$$+\begin{bmatrix} a_{13}(\varepsilon_1, \varepsilon_2) & a_{14}(\varepsilon_1, \varepsilon_2) \\ a_{23}(\varepsilon_1, \varepsilon_2) & a_{24}(\varepsilon_1, \varepsilon_2) \end{bmatrix}\begin{Bmatrix} z_3 \\ z_4 \end{Bmatrix}+\begin{Bmatrix} \alpha\bar{\Omega}_1^2\left[\dfrac{\xi}{d}z_1(z_1^2+z_2^2)-\dfrac{\eta}{d}z_2(z_1^2+z_2^2)\right]+e_1(\mathbf{z}, \mathbf{y}_2) \\ \alpha\bar{\Omega}_1^2\left[\dfrac{\eta}{d}z_1(z_1^2+z_2^2)+\dfrac{\xi}{d}z_2(z_1^2+z_2^2)\right]+e_2(\mathbf{z}, \mathbf{y}_2) \end{Bmatrix}, \tag{36a}$$

$$\begin{Bmatrix} \dot{z}_3 \\ \dot{z}_4 \end{Bmatrix}=\begin{bmatrix} \xi+\eta\mathrm{i} & 0 \\ 0 & \xi-\eta\mathrm{i} \end{bmatrix}\begin{Bmatrix} z_3 \\ z_4 \end{Bmatrix}$$

$$+\begin{bmatrix} \bar{\Omega}_1\varepsilon_1+\dfrac{\mathrm{i}\bar{\Omega}_1}{2(1+2\mathscr{M})}\varepsilon_2+b_3 & \dfrac{\bar{\Omega}_1}{2(1+2\mathscr{M})}\varepsilon_2-\mathrm{i}\bar{\Omega}_1\varepsilon_1+b_4 \\ \mathrm{i}\bar{\Omega}_1\varepsilon_1-\dfrac{\bar{\Omega}_1}{2(1+2\mathscr{M})}\varepsilon_2-b_4 & \bar{\Omega}_1\varepsilon_1-\dfrac{\mathrm{i}\bar{\Omega}_1}{2(1+2\mathscr{M})}\varepsilon_2+\bar{b}_3 \end{bmatrix}\begin{Bmatrix} z_1 \\ z_2 \end{Bmatrix}$$

$$+\begin{bmatrix} a_{33}(\varepsilon_1, \varepsilon_2) & a_{34}(\varepsilon_1, \varepsilon_2) \\ a_{43}(\varepsilon_1, \varepsilon_2) & a_{44}(\varepsilon_1, \varepsilon_2) \end{bmatrix}\begin{Bmatrix} z_3 \\ z_4 \end{Bmatrix}+\begin{Bmatrix} e_3(\mathbf{z}, \mathbf{y}_2) \\ e_4(\mathbf{z}, \mathbf{y}_2) \end{Bmatrix}. \tag{36b}$$

In addition to equations (36a) and (36b), the other governing equations are

$$\dot{\mathbf{y}}_2=[\mathbf{C}_{20}+\mathbf{C}_{21}+\mathbf{C}_{22}]\mathbf{y}_2+\mathbf{n}_2(\mathbf{Qz},\mathbf{y}_2),\qquad \dot{\underline{\varepsilon}}=\begin{Bmatrix}\dot{\varepsilon}_1\\ \dot{\varepsilon}_2\end{Bmatrix}=\begin{Bmatrix}0\\0\end{Bmatrix}. \tag{36c, d}$$

In equations (36a) and (36b), b_1, b_2, b_3 and b_4 are quadratic functions of ε_1 and ε_2 of the forms

$$b_1=-\frac{\xi}{d}\varepsilon_1^2-\frac{\eta}{d}\frac{\varepsilon_1\varepsilon_2}{(1+2\mathscr{M})},\qquad b_2=\frac{\eta\varepsilon_1^2}{d}-\frac{\xi}{d}\frac{\varepsilon_1\varepsilon_2}{(1+2\mathscr{M})},$$

$$b_3=\frac{\varepsilon_1^2}{2}+\frac{\mathrm{i}\varepsilon_1\varepsilon_2}{2(1+2\mathscr{M})},\qquad b_4=\frac{\varepsilon_1\varepsilon_2}{2(2+2\mathscr{M})}-\frac{\mathrm{i}\varepsilon_1^2}{2}; \tag{37}$$

$\bar{b}_3$ is the complex conjugate of b_3; a_{13}, a_{14}, $\cdots$, a_{44} are the elements of the matrix $\mathbf{A}=\mathbf{Q}^{-1}\mathbf{C}_{1\varepsilon}\mathbf{Q}$ and are quadratic functions of ε_1 and ε_2 with zero values at $\varepsilon_1=\varepsilon_2=0$; e_1, e_2, e_3 and e_4 are high order terms in the variables $\mathbf{z}$ and $\mathbf{y}_2$.

By center manifold theory it is known that there exists a center manifold for equations (36), $(z_3, z_4, \mathbf{y}_2^{\mathrm{T}})^{\mathrm{T}}=\mathbf{h}(z_1, z_2, \underline{\varepsilon})$, $|z_1|\leqslant\delta$, $|z_2|\leqslant\delta$, $|\underline{\varepsilon}|\leqslant\delta$, where the vector $\mathbf{h}$ is C^2. For simplicity one can write $\mathbf{x}_1=(z_1, z_2)^{\mathrm{T}}$, $\mathbf{x}_2=(z_3, z_4)^{\mathrm{T}}$, and rewrite equations (36a) and (36b) in the forms

$$\dot{\mathbf{x}}_1=\mathbf{A}_1(\underline{\varepsilon})\mathbf{x}_1+\mathbf{A}_2(\underline{\varepsilon})\mathbf{x}_2+\underline{\boldsymbol{\beta}}_1(\mathbf{z},\mathbf{y}_2), \tag{38a}$$

$$\dot{\mathbf{x}}_2=\mathbf{B}_0\mathbf{x}_2+\mathbf{B}_1(\underline{\varepsilon})\mathbf{x}_1+\mathbf{B}_2(\underline{\varepsilon})\mathbf{x}_2+\underline{\boldsymbol{\beta}}_2(\mathbf{z},\mathbf{y}_2). \tag{38b}$$

Denoting $\mathbf{h}_1=(h_3, h_4)^{\mathrm{T}}$ and $\mathbf{h}_2=(h_5, h_6, h_7, h_8)^{\mathrm{T}}$, substituting $(z_3, z_4, \mathbf{y}_2^{\mathrm{T}})^{\mathrm{T}}=\mathbf{h}(\mathbf{x}_1, \underline{\varepsilon})=(\mathbf{h}_1^{\mathrm{T}}, \mathbf{h}_2^{\mathrm{T}})^{\mathrm{T}}$ into equations (38a) and (38b), and using the chain rule, one obtains

$$(M_0\mathbf{h}_1)(\mathbf{x}_1, \underline{\varepsilon})=\frac{\partial(h_3, h_4)}{\partial\mathbf{x}_1}[\mathbf{A}_1(\underline{\varepsilon})\mathbf{x}_1+\mathbf{A}_2(\underline{\varepsilon})\mathbf{h}_1+\underline{\boldsymbol{\beta}}_1(\mathbf{h}_1, \mathbf{h}_2)]$$
$$-\mathbf{B}_0\mathbf{h}_1-\mathbf{B}_1(\underline{\varepsilon})\mathbf{x}_1-\underline{\mathbf{B}_2(\underline{\varepsilon})\mathbf{h}_1}-\underline{\boldsymbol{\beta}}_2(\mathbf{h}_1, \mathbf{h}_2)=0, \tag{39a}$$

$$(M_0\mathbf{h}_2)(\mathbf{x}_1, \underline{\varepsilon})=\frac{\partial(h_5, \ldots, h_8)}{\partial\mathbf{x}_1}[\mathbf{A}_1(\underline{\varepsilon})\mathbf{x}_1+\mathbf{A}_2(\underline{\varepsilon})\mathbf{h}_1+\underline{\boldsymbol{\beta}}_1(\mathbf{h}_1, \mathbf{h}_2)]$$
$$-\mathbf{C}_{20}\mathbf{h}_2+[\mathbf{C}_{21}+\mathbf{C}_{22}]\mathbf{h}_2+\underline{\mathbf{n}_2(\mathbf{h}_1, \mathbf{h}_2)}=0. \tag{39b}$$

The partial differential equation for $\mathbf{h}$ cannot be solved explicitly but can be approximated arbitrarily well by a Taylor series near $(\mathbf{x}_1, \underline{\varepsilon})^{\mathrm{T}}=\mathbf{0}$, provided that its Taylor series exists. Carr [16] showed that if the function $\underline{\boldsymbol{\phi}}(\mathbf{x}_1, \underline{\varepsilon})=O(|\mathbf{x}_1, \varepsilon|^p)$ for some $p>1$ as $|\mathbf{x}_1, \underline{\varepsilon}|\to 0$, then it follows that

$$|\mathbf{h}(\mathbf{x}_1, \underline{\varepsilon})-\underline{\boldsymbol{\phi}}(\mathbf{x}_1, \underline{\varepsilon})|=O(|\mathbf{x}_1, \underline{\varepsilon}|^p)\qquad \text{as } |\mathbf{x}_1, \underline{\varepsilon}|\to 0. \tag{40}$$

Hence one can approximate $\mathbf{h}$ as closely as desired by seeking series solutions of equation (39). Since the center manifold is tangent to the z_1–z_2 plane at the origin, the power series for $\mathbf{h}$ must begin with quadratic terms. Since the underlined terms in equation (39a) are of $O(|\mathbf{x}_1, \underline{\varepsilon}|^3)$ and the last term is of $O|\mathbf{x}_1, \underline{\varepsilon}|^4$, one chooses $(\phi_3, \phi_4)^{\mathrm{T}}$ such that

$$\mathbf{B}_0(\underline{\varepsilon})\begin{Bmatrix}\phi_3\\ \phi_4\end{Bmatrix}-\mathbf{B}_1^*(\underline{\varepsilon})\mathbf{x}_1=0, \tag{41}$$

where $\mathbf{B}_1^*$ is the matrix $\mathbf{B}_1$ with the second order terms b_4 and $\bar{b}_3$ removed. The solution of equation (41) is

$$\begin{Bmatrix}\phi_3\\ \phi_4\end{Bmatrix}=\frac{1}{d}\begin{bmatrix}\xi-\eta\mathrm{i} & 0\\ 0 & \xi+\eta\mathrm{i}\end{bmatrix}\mathbf{B}_1^*(\underline{\varepsilon})\begin{Bmatrix}z_1\\ z_2\end{Bmatrix}. \tag{42}$$

ϕ_3 and ϕ_4 are quadratic functions of $\mathbf{x}_1$ and $\underline{\varepsilon}$. So

$$\begin{Bmatrix}z_3\\ z_4\end{Bmatrix}=\begin{Bmatrix}h_3\\ h_4\end{Bmatrix}=\begin{Bmatrix}\phi_3\\ \phi_4\end{Bmatrix}+O(|\mathbf{x}_1,\underline{\varepsilon}|^3),\qquad \begin{Bmatrix}(M_0\phi_3)\\ (M_0\phi_4)\end{Bmatrix}=O(|\mathbf{x}_1,\underline{\varepsilon}|^3). \tag{43}$$

Similarly, if $\underline{\Phi}_2=(\phi_5,\ldots,\phi_8)^{\mathrm{T}}$ is of $O(|\mathbf{x}_1,\underline{\varepsilon}|^q)$, the underlined terms in equation (39b) are at least one order higher than q but the term $\mathbf{C}_{20}\underline{\Phi}_2$ is of order q. So

$$\mathbf{y}_2=\mathbf{h}_2=\underline{\Phi}_2=\mathbf{0}. \tag{44}$$

Substituting equations (43) and (44) into equation (36a), one has

$$\begin{Bmatrix}\dot{z}_1\\ \dot{z}_2\end{Bmatrix}=\begin{bmatrix}-\frac{\xi}{d}2\bar{\Omega}_1\varepsilon_1-\frac{\eta\bar{\Omega}_1}{d(1+2\mathscr{M})}\varepsilon_2+b_1 & \frac{\eta}{d}2\bar{\Omega}_1\varepsilon_1-\frac{\xi\bar{\Omega}_1}{d(1+2\mathscr{M})}\varepsilon_2+b_2\\ -\frac{\eta}{d}2\bar{\Omega}_1\varepsilon_1+\frac{\xi\bar{\Omega}_1}{d(1+2\mathscr{M})}\varepsilon_2-b_2 & -\frac{\xi}{d}2\bar{\Omega}_1\varepsilon_1-\frac{\eta\bar{\Omega}_1}{d(1+2\mathscr{M})}\varepsilon_2+b_1\end{bmatrix}\begin{Bmatrix}z_1\\ z_2\end{Bmatrix} \tag{45}$$

$$+\begin{bmatrix}f_{11}(\varepsilon_1,\varepsilon_2) & f_{12}(\varepsilon_1,\varepsilon_2)\\ f_{21}(\varepsilon_1,\varepsilon_2) & f_{22}(\varepsilon_1,\varepsilon_2)\end{bmatrix}\begin{Bmatrix}z_1\\ z_2\end{Bmatrix}+\alpha\bar{\Omega}_1^2\begin{Bmatrix}\frac{\xi}{d}z_1(z_1^2+z_2^2)-\frac{\eta}{d}z_2(z_1^2+z_2^2)\\ \frac{\eta}{d}z_1(z_1^2+z_2^2)+\frac{\xi}{d}z_2(z_1^2+z_2^2)\end{Bmatrix}+O(|\mathbf{x}_1,\underline{\varepsilon}|^4),$$

where the functions f_{11}, f_{12}, f_{21}, and f_{22} are of $O(|\underline{\varepsilon}|^2)$.

Upon introducing polar co-ordinates $z_1=r\cos\theta$, $z_2=r\sin\theta$ and neglecting b_1, b_2, f_{11}, f_{12}, f_{21}, f_{22} and higher order terms, equation (45) becomes

$$\dot{r}=\left\{\left[-\frac{\xi}{d}2\bar{\Omega}_1\varepsilon_1-\frac{\eta\bar{\Omega}_1}{d(1+2\mathscr{M})}\varepsilon_2\right]+\alpha\bar{\Omega}_1^2\frac{\xi}{d}r^2\right\}r, \tag{46a}$$

$$\dot{\theta}=\left\{\left[-\frac{\eta}{d}2\bar{\Omega}_1\varepsilon_1+\frac{\xi\bar{\Omega}_1}{d(1+2\mathscr{M})}\varepsilon_2\right]+\alpha\bar{\Omega}_1^2\frac{\eta}{d}r^2\right\}. \tag{46b}$$

Equations (46) are valid only in the neighborhood of the point D. Some results revealed by equation (46) can be summarized as follows.

(1) For the case $\varepsilon_2=0$ which corresponds to zero external damping, the zero solution (pure undeformed rotation of the shaft-disk system) is asymptotically stable (unstable) if $\varepsilon_1<0$ ($\varepsilon_1>0$) since ξ given by equation (27) is always negative. For the case $\mu_e=\varepsilon_1=0$ (that is, the exact point D in Figure 2) the zero solution is stable since the coefficient of the r^3 term in equation (46a) is negative, but the linear analysis in section 3 predicts incorrectly a first mode whirling. A non-trivial circle of equilibria, which bifurcates from the trivial solution at $\varepsilon_1=0$, exists and is stable for $\varepsilon_1>0$. From equation (46a) the radius of the circle of equilibria is

$$r=\sqrt{2(\Omega-\bar{\Omega}_1)}/\alpha\bar{\Omega}_1, \tag{47}$$

which is independent of the internal damping. Also one has $\dot{\theta}=0$ from equation (46b), which indicates that the first mode is whirling synchronously. Equation (30) indicates that

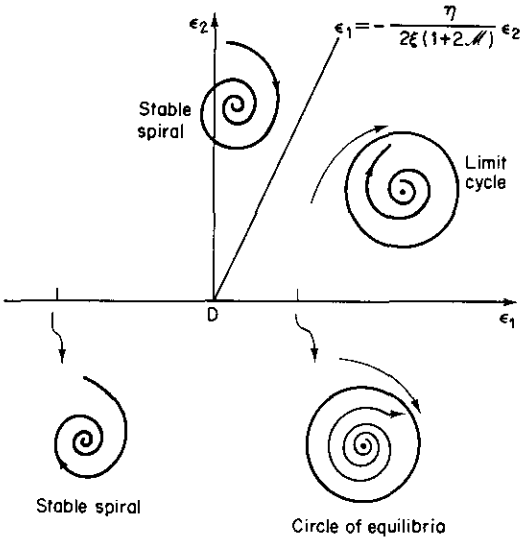

Figure 3. Bifurcation diagram and associated phase portraits of equation (45).

the radius of the first mode whirling is

$$R_1 = \sqrt{(\Omega+\bar{\Omega}_1)(\Omega-\bar{\Omega}_1)}/\alpha\bar{\Omega}_1^2 \simeq \sqrt{2(\Omega-\bar{\Omega}_1)}/\alpha\bar{\Omega}_1, \tag{48}$$

where the approximations $\Omega \simeq \bar{\Omega}_1$ and $\Omega+\bar{\Omega}_1 \simeq 2\bar{\Omega}_1$ have been used, since $\varepsilon_1 = \Omega - \bar{\Omega}_1 > 0$ is very small in the neighborhood of the point D. Comparing equation (48) with equation (47) shows that the center manifold theory predicts the correct radius of the circle of equilibria.

(2) For the case $\varepsilon_2 \neq 0$, a supercritical Hopf bifurcation is found on those points in the ε_1-ε_2 plane where $\varepsilon_1 = -\eta\varepsilon_2/[2\xi(1+2\mathcal{M})]$. The zero solution loses its stability and bifurcates into a family of stable periodic orbits (limit cycle solutions) for $\varepsilon_1 > -\eta\varepsilon_2/[2\xi(1+2\mathcal{M})]$. The radius of the limit cycle is determined by the equation

$$[-(\xi/d)2\bar{\Omega}_1\varepsilon_1 - \{\eta\bar{\Omega}_1/d(1+2\mathcal{M})\}\varepsilon_2] + \alpha\bar{\Omega}_1^2(\xi/d)r^2 = 0.$$

Thus

$$r^2 = \{2(\sqrt{1+2\mathcal{M}}\Omega - \Omega_1)/\alpha\Omega_1\} - \{2\mu_e/\alpha\mu_i\Omega_1^2\}. \tag{49}$$

Equation (49) reveals that the radius is proportional to the square root of the rotational speed (i.e., to $\sqrt{\Omega}$), decreases as the external damping increases, and increases as the internal damping increases. The substitution of equation (49) into equation (46b) yields

$$\dot{\theta} = -\mu_e/\mu_i\Omega_1\sqrt{1+2\mathcal{M}}. \tag{50}$$

Since $\dot{\theta} \neq 0$, non-synchronous whirling of the first mode arises in this case. This phenomenon was observed in Newkirk's experiment [19]. The whirling speed of the shaft-disk system is given by $\Omega_{whirl} = \Omega + \dot{\theta}$. Equation (50) reveals that the precession rate $\dot{\theta}$ of the shaft is linearly proportional to the external damping, inversely proportional to the internal damping, and independent of the spin rate Ω. The bifurcation set and the associated phase portraits of equation (46) are shown in Figure 3.

4.3. NUMERICAL SOLUTION AND DISCUSSION

The non-intersection points on the stability boundaries, such as the points 3 and 7 in Figure 2, have one pair of imaginary eigenvalues; therefore simple Hopf bifurcation of a

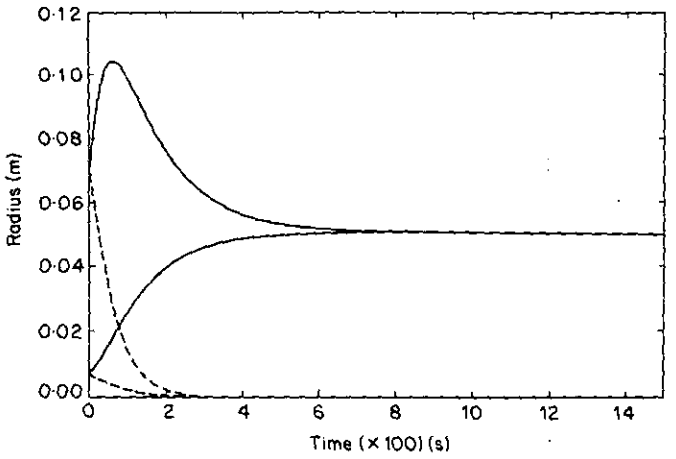

Figure 4. Time history of R_1 at $x=l/2$ and R_2 at $x=l/4$ for point 1. ——, $R_1=(v_1^2+w_1^2)^{1/2}$; – – –, $R_2=(v_2^2+w_2^2)^{1/2}$.

periodic orbit from the zero solution is expected. At the intersection point 6 two pairs of pure imaginary eigenvalues coexist, and this suggests the existence of a double Hopf bifurcation. Essentially, center manifold theory may be applied to study the qualitative behavior near these points, but it is bypassed here due to the complexity. Instead, numerical simulations based on equation (15) are employed only typical points on the stability boundaries and in the regions II, III and IV of Figure 2.

Since point 1 ($\mu_e=0$, $\Omega=10$ in region II) is below the stability boundary defined by equation (26), the second mode motion will approach zero and the non-trivial steady state solution will exist according to the analysis of section 4.1. The time history of the radii $R_1=\sqrt{v_1^2(t)+w_1^2(t)}$ for the first mode and $R_2=\sqrt{v_2^2(t)+w_2^2(t)}$ for the second mode are shown in Figure 4. The second mode motion indeed tends to zero as predicted theoretically. At steady state the radius of the circle of equilibria, that is R_1, is of the same value as predicted by equation (30) and is independent of the initial conditions chosen. Figure 5 is the phase diagram for the variable v_1, which reveals that the shaft–disk system is finally in the steady state as $\dot{v}_1$ approaches zero.

Point 2 ($\mu_e=0$, $\Omega=56$) is in region IV, so the motion of the first mode or the second mode may exist according to the result of section 4.1. The numerical solutions show that the shaft–disk system is always in the synchronous first-mode whirling as $t\to\infty$ from any

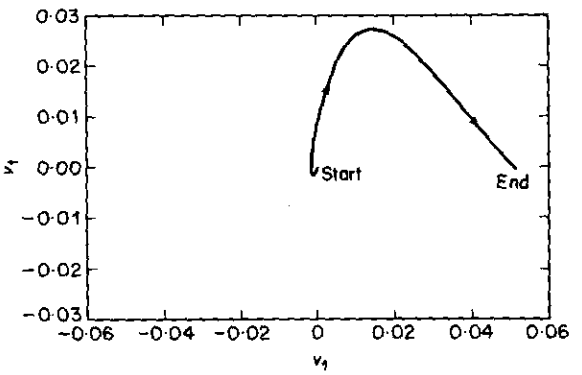

Figure 5. The v_1–$\dot{v}_1$ phase diagram for point 1.

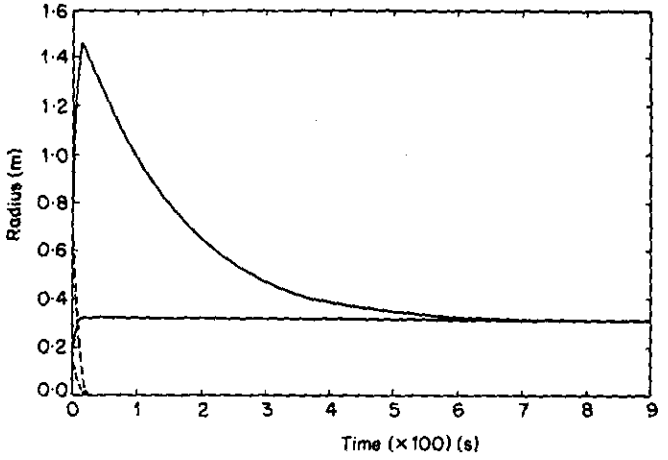

Figure 6. $R_1(l/2, t)$ and $R_2(l/4, t)$ for point 2. Key as Figure 4.

set of initial conditions except the initial condition of the exact second-mode shape which induces the synchronous second-mode whirling. The time histories of R_1 and R_2 for two sets of initial conditions are shown in Figure 6, in which the R_2 representing the second mode motion dies out rapidly. The value of the radius R_1 is the same as that estimated by equation (31a).

Point 3 ($\mu_e = 400$, $\Omega = 24{\cdot}59$) is on the stability boundary, its instability cannot be determined by the linear analysis. The numerical solution as shown in Figure 7 indicates that the motion is asymptotically stable.

Point 5 ($\mu_e = 400$, $\Omega = 60$) is in the same region IV as point 2. It is shown in Figure 8 that after a long period only the non-synchronous first-mode whirling persists for the two sets of mixed first-mode and second-mode initial conditions. The non-synchronous second-mode whirling, as shown in Figure 9, exists only if the initial conditions of the exact second-mode shape are assigned. The result of section 4.1 indicates that the non-trivial steady state solution does not exist when $\mu_e = 0$. The numerical solution indicates that the motion is a limit cycle which is illustrated by the v_1, $\dot{v}_1$ phase diagram shown in Figure 10. The trajectory, measured from the rotating x, y, z co-ordinates, of the variables v_1 and

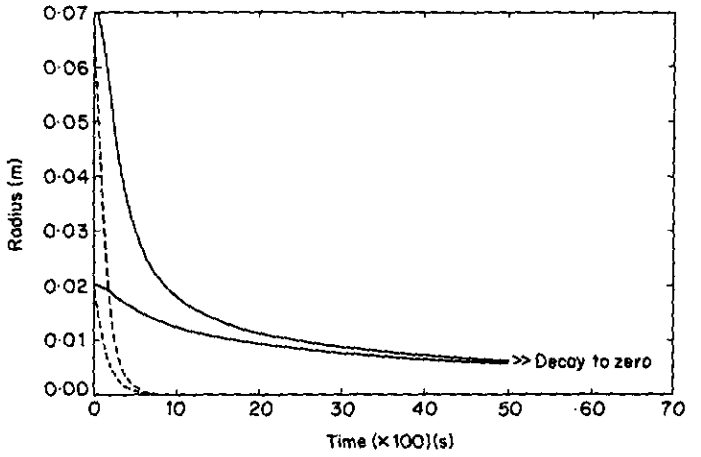

Figure 7. $R_1(l/2, t)$ and $R_2(l/4, t)$ for point 3. Key as Figure 4.

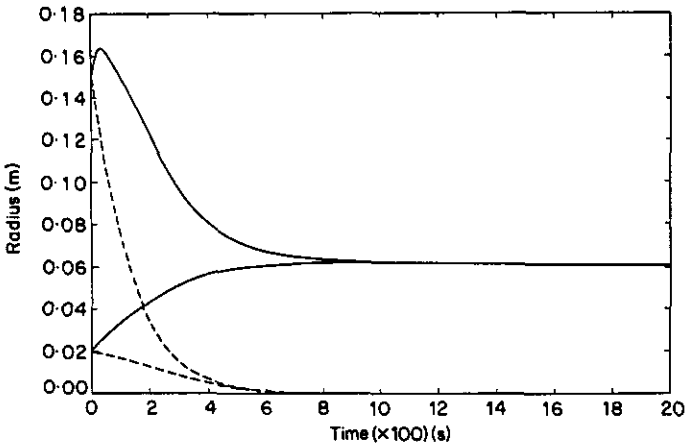

Figure 8. $R_1(l/2, t)$ and $R_2(l/4, t)$ for point 5. Key as Figure 4.

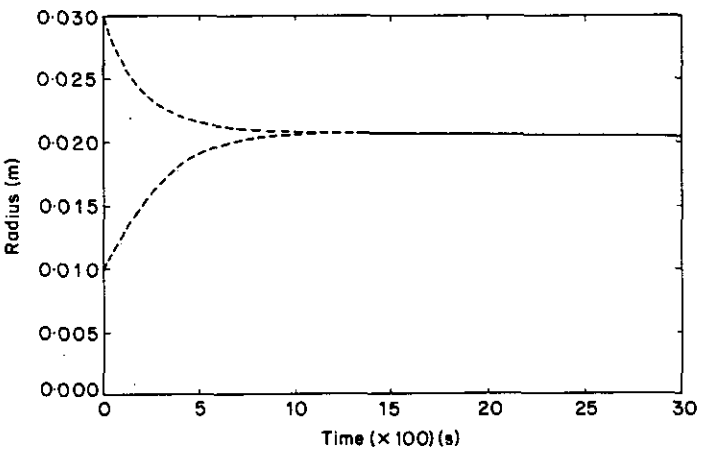

Figure 9. Time history of R_2 ($x=l/2$) for point 5 with the initial condition that of the exact second mode shape. - - -, $R_2=(v_2^2+w_2^2)^{1/2}$.

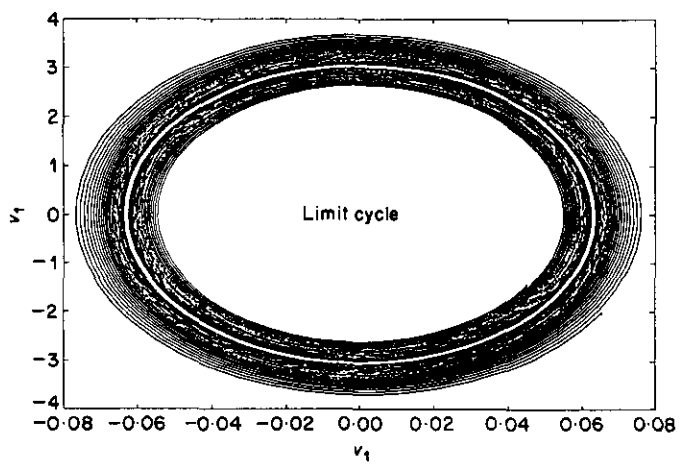

Figure 10. Phase portrait in v_1–$\dot{v}_1$ space for point 5.

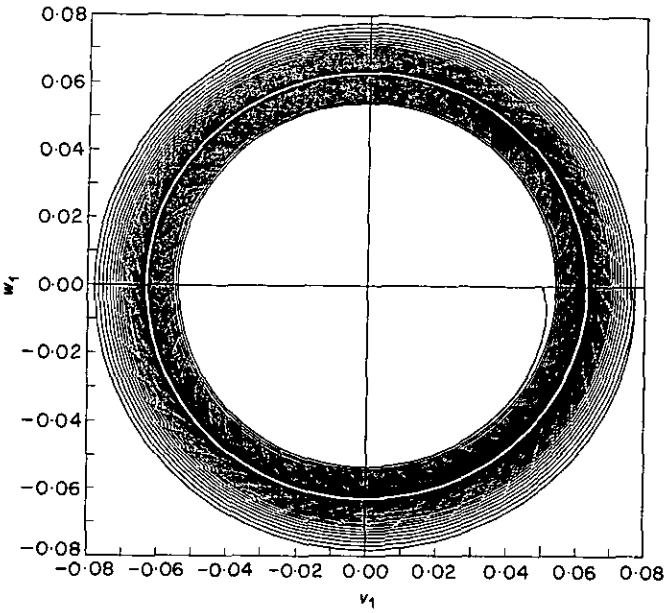

Figure 11. Trajectory for v_1 and w_1 at $x=l/2$ for point 5.

w_1 at $x=l/2$ approaches counter-clockwise the limit cycle from an initial position either inside or outside the limit cycle, as shown in Figure 11. This reveals that the shaft–disk system does not synchronize with the x, y and z co-ordinates but with an angular velocity lag (or a negative precession rate). The relation between the precession rate $\dot{\theta}$ and the rotational speed Ω with μ_e fixed is shown in Figure 12, which indicates that $\dot{\theta}$ is proportional to Ω. This is different from the behavior at those points near the point D, where $\dot{\theta}$ does not depend on Ω, as shown by equation (50). The relation between $\dot{\theta}$ and the external damping is shown in Figure 13. It is clear that $\dot{\theta}$ is not linearly proportional to μ_e, as equation (50) indicates. Therefore the effects of the system parameters on $\dot{\theta}$ for points outside and away from the stability boundaries is somewhat different from those for points near the point D. The effects of the parameters Ω, μ_i and μ_e on the radius of the limit cycle are shown in Figures 14–16, which are similar qualitatively to those for points near the point D as predicted by equation (49). Point 4 ($\mu_e=400$, $\Omega=36$) is in the same region

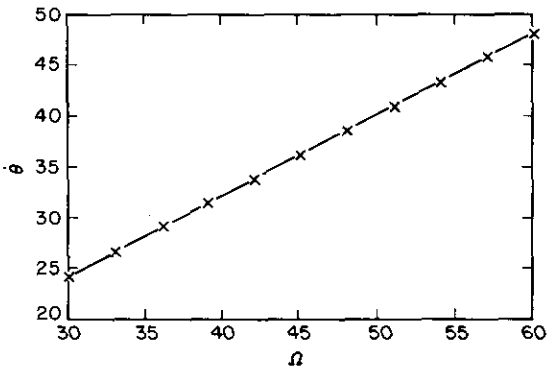

Figure 12. The precession rate $\dot{\theta}$ as a function of the rotational speed Ω for fixed $\mu_e=400$.

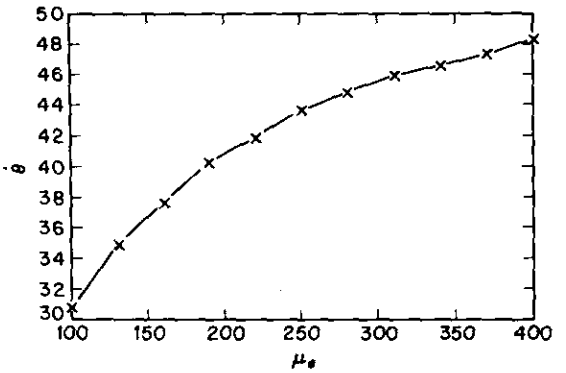

Figure 13. $\dot{\theta}$ as a function of μ_e for fixed $\Omega = 60$.

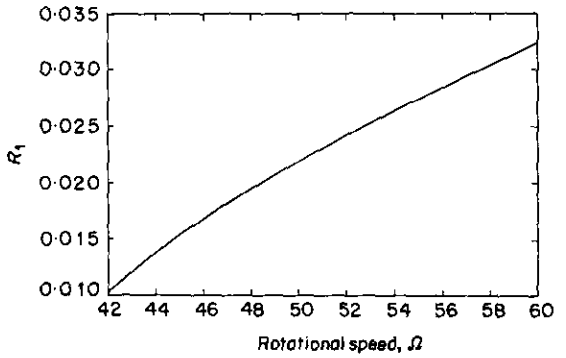

Figure 14. The radius R_1 ($x = l/2$) of the first-mode limit cycle as a function of Ω for fixed $\mu_e = 400$.

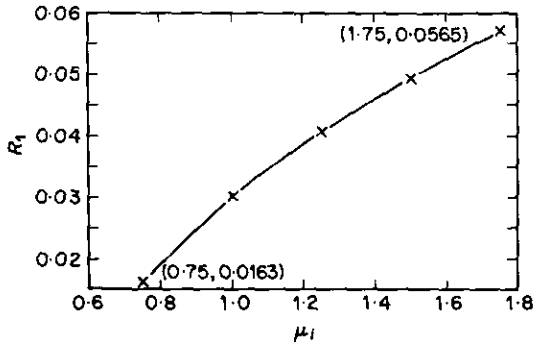

Figure 15. R_1 ($x = l/2$) as a function of μ_i for $\mu_e = 400$ and $\Omega = 60$.

II as point 1. The second-mode motion will die out and the limit cycle motion of the first mode is similar to that of point 5.

The solutions for point 6 ($\mu_e = 1044{\cdot}95$, $\Omega = 56{\cdot}48$) and point 7 ($\mu_e = 1200$, $\Omega = 57{\cdot}45$) are asymptotically stable. The time history of R_1 at $x = l/2$ and R_2 at $x = l/4$ for point 6 is shown in Figure 17. According to the numerical experiment the motions of the points on the stability curves are asymptotically stable.

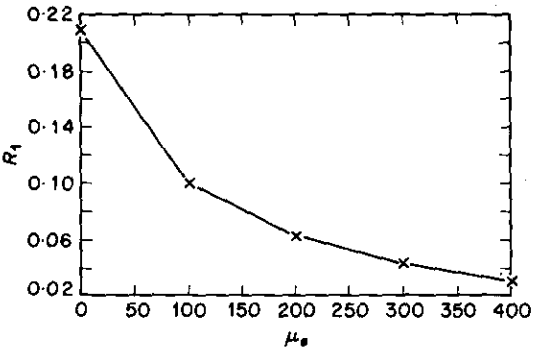

Figure 16. R_1 $(x=l/2)$ as a function of μ_e for $\Omega=60$.

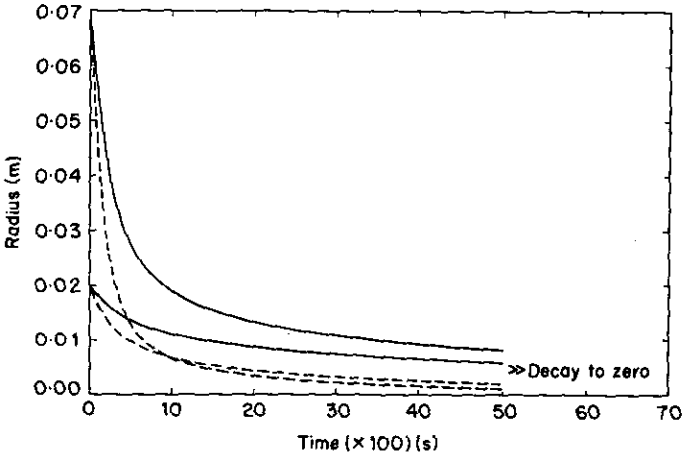

Figure 17. Time history of R_1 $(x=l/2)$ (——) and R_2 $(x=l/4)$ (– – –) for point 6.

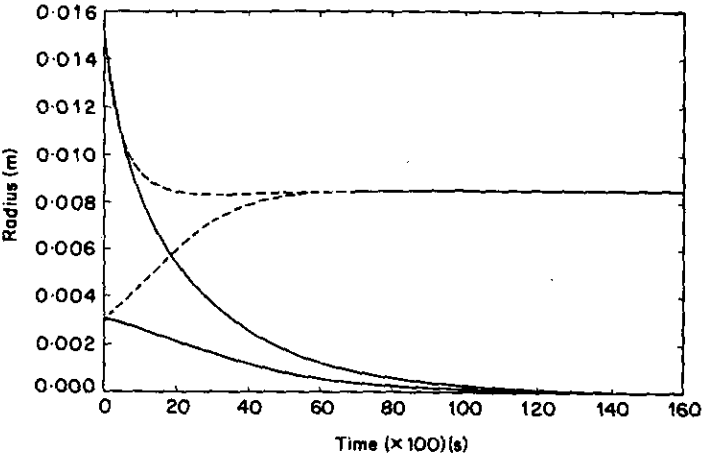

Figure 18. Time history of R_1 $(x=l/2)$ (——) and R_2 $(x=l/4)$ for point 8.

Point 8 ($\mu_e = 1200$, $\Omega = 60$) is in region III which is below the stability curve of equation (22) and above the stability curve of equation (26), so the first mode motion will die out and the second mode motion will persist. The time history of R_1 at $x = l/2$ and R_2 at $x = l/4$ is shown in Figure 18.

Point 9 ($\mu_e = 1200$, $\Omega = 76$) is in the same region IV as point 5. The first mode motion can be excited only if the initial conditions of the exact first mode shape are assigned; otherwise only the limit cycle motion of the second mode can exist. This means that for large external damping first mode whirling is not easily induced.

5. CONCLUSIONS

The linear equations of motion, based on the assumption of small deformation, predict that the undeformed rotating state of a shaft–disk system will lose its stablity when the rotational speed is higher than the critical speeds. If the viscoelastic shaft is allowed to experience large deformation, the non-linear equations of motion will predict (neutrally) stable motion for the shaft–disk system even if the rotational speed is far above the critical speeds. By the use of center manifold theory we have shown the existence of synchronous post-critical whirling for the case of non-zero external damping, which are in accord with experimental results in the existing literature. The precession rate of the shaft and the radius of the limit cycle near the double zero eigenvalue bifurcation point have been obtained analytically in explicit form.

REFERENCES

1. A. L. KIMBALL 1924 *General Electric Review* **17**, 244–251. Internal friction theory of shaft whirlings.
2. V. V. BOLOTIN 1963 *Nonconservative Problems of the Theory of Elastic Stability*. New York: Pergamon Press.
3. F. F. EHRICH 1964 *Journal of Applied Mechanics* **31**, 279–282. Shaft whirl induced by rotor internal damping.
4. J. GENIN and J. S. MAYBEE 1971 *Journal of Sound and Vibration* **21**, 399–404. The role of material damping in the stability of rotation systems.
5. B. J. TORBY 1979 *Journal of Applied Mechanics* **46**, 469–470. The effect of structural damping upon the whirling of rotors.
6. L. L. BUCCIARELLI 1982 *Journal of Applied Mechanics* **49**, 425–428. On the instability of rotating shafts due to internal damping.
7. W. ZHANG and F. H. LING 1986 *Journal of Applied Mechanics* **53**, 424–429. Dynamic stability of the rotating shaft made of Boltzmann viscoelastic solid.
8. S. L. HENDRICKS 1986 *Journal of Applied Mechanics* **53**, 412–416. The effect of viscoelasticity on the vibration of a rotor.
9. L. MEIROVITCH and G. RYLAND 1985 *Journal of Sound and Vibration* **100**, 393–408. Perturbation technique for gyroscopic systems with small internal and external damping.
10. K. WASHIZU 1982 *Variational Method in Elasticity and Plasticity*. New York: Pergamon Press, third edition.
11. C. H. HO, R. A. SCOTT and J. G. EISLEY 1975 *International Journal of Nonlinear Mechanics* **10**, 113–127. Non-planar nonlinear oscillations of a beam—I, forced motions.
12. J. D. ACHENBACH 1973 *Wave Propagation in Elastic Solids*. Amsterdam: North-Holland. See pp. 63–65.
13. C. O. CHANG, M. L. TSAI and C. S. CHOU 1992 *Journal of Sound and Vibration* **153**, 259–289. On the viscoelastic beam damper for a freely precessing gyroscope.
14. B. J. LAZAN 1968 *Damping of Materials and Members in Structural Mechanics*. New York: Pergamon Press.

15. L. MEIROVITCH 1980 *Computational Methods in Structural Dynamics*. Alphen aan der Rijn: Sijthoff & Noordhoff.
16. J. CARR 1981 *Applications of Center Manifold Theory*. New York: Springer-Verlag.
17. S. WOLFRAM 1988 *Mathematica*. New York: Addison-Wesley.
18. J. GUCKENHEIMER and P. HOLMES 1983 *Nonlinear Oscillation, Dynamical Systems, and Bifurcation of Vector Fields*. New York: Springer-Verlag.
19. B. L. NEWKIRK 1924 *General Electric Review* **27**, 169–178. Shaft whipping.